The steadfast Au@Pt soldier: Peroxide-tolerant nanozyme for signal enhancement in lateral flow immunoassay of peroxidase-containing samples

Vasily G. Panferov, Irina V. Safenkova, Anatoly V. Zherdev, Boris B. Dzantiev*

A.N. Bach Institute of Biochemistry, Research Center of Biotechnology of the Russian Academy of Sciences, Leninsky prospect 33, 119071 Moscow, Russia

* corresponding author – dzantiev@inbi.ras.ru

Graphical abstract

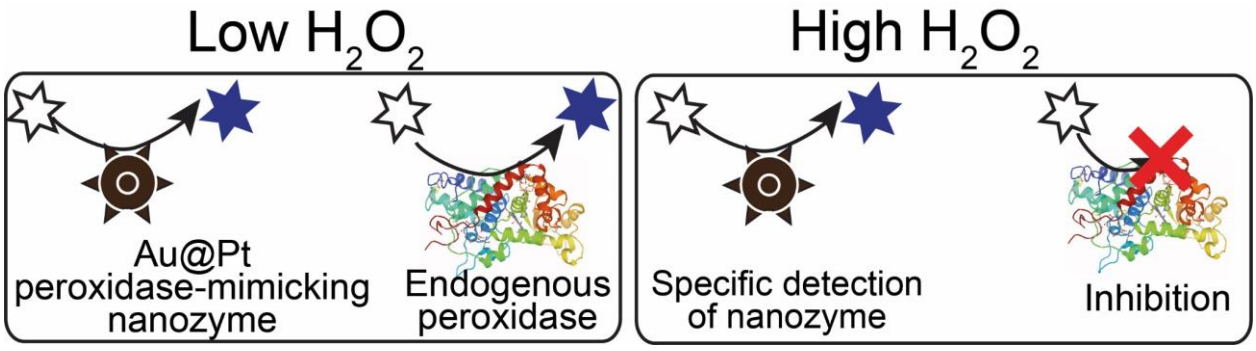

Abstract. We report the approach for the detection of Au@Pt core@shell nanoparticles (nanozymes) with peroxidase-mimicking activity (PMA) in samples with high endogenous peroxidase activity (EPA). Unlike the endogenous peroxidases in plant extracts that are inhibited by elevated H_2O_2 (>20 mM), the PMA of nanozymes was stable in concentrated H_2O_2 (up to 4 M). Such a different stability of enzymes and Au@Pt to the substrate allowed for eliminating EPA and detecting only nanozymes. The developed approach was used for reaching a lower limit of detection (LOD) and eliminating the background for the lateral flow immunoassay (LFIA) of the important plant pathogen potato virus X (PVX) in leaf and tuber extracts. Using the PMA of Au@Pt, the LOD was reduced to 4 and 8 pg/mL in tuber and leaf extracts, respectively. The LOD values are 250- and 500-times lower in comparison with LFIA with conventional gold nanoparticles. The developed approach of peroxidases inhibition is universal for bioanalytical methods, and its applicability was confirmed by the elimination of EPA in three matrixes (serum, potato leaf and tuber extracts).

Key words: peroxidase-mimicking; endogenous peroxidase; artificial peroxidase; enzyme-mimicking; enzyme inhibition; limit of detection; core@shell nanoparticles; nanocatalyst; plant pathogens.

Introduction

Nanozymes are nanoparticles possessing enzyme-mimicking activity. At the moment, nanozymes with peroxidase, oxidase, catalase, superoxide dismutase and hydrolase activities are reported.[1] Among them, nanozymes with peroxidase-mimicking activity (PMA) have a broad application in different bioassays as the optical/catalytic labels and nanosized carriers of receptor biomolecules.[2] Tunable catalytic activity [3] (comparable or even higher than for enzymes [4]), well-developed protocols of synthesis/functionalization [5] and multifunctionality make nanozymes promising tools for bioanalytical chemistry.

In comparison with enzymes, nanozymes possess a higher stability of PMA in the broad ranges of pH, temperature and concentrations of inhibitors.[6] Although such stability of PMA was shown for ferromagnetic nanoparticles in a pioneer article by Gao [7] and has since been reported repeatedly for different nanozymes, it has not been found to have practical implementation in scientific articles neither commercial bioanalytical assays. Thus, a trump card of nanozymes remains unrealized.

We suggest the use of a high-stability of nanozymes' PMA for overcoming the background signals arising from endogenous peroxidase activity (EPA). EPA leads to false-positive results for assays using horseradish peroxidase (HRP) as the label. High EPA even affects the assays (ELISA) with multiple washing.[8] Nevertheless, EPA is especially critical for the wash-free point-of-care methods, which detect the label in the background of peroxidases.[9] Overcoming this limitation will provide a wider application of nanozymes as labels for point-of-care assays.

Proposed in this article is an approach that utilizes a higher stability of nanozymes' PMA in concentrated H_2O_2. Nanozymes remain catalytic-active, while peroxidases in matrixes are inhibited by the elevated H_2O_2 concentrations (i.e. substrate inhibition). Despite the fact that this approach is widely used for histochemical studies [10,11] it has not been applied to the highly sensitive point-of-care immunochemical assays.

We selected lateral flow immunoassay (LFIA) to demonstrate the applicability of the proposed approach. LFIA is a point-of-care method that combines the formation of complexes between antigen and antibodies and the affine separation of these complexes using porous membranes. For the detection of immune complexes, antibodies are conjugated to the different nanosized labels.[12] Despite the simplicity and rapidity of LFIA, a high limit of detection (LOD) limits the applicability of the assay.[13] Using nanozymes as the catalytic label, significant reduction of the LOD of LFIA is achieved through the increase of the colourimetric signal caused by the accumulation of an insoluble coloured product.[13] However, the application of

nanozymes as catalytic labels in LFIA is still limited. Because conventional LFIA is a wash-free method, nanozymes are detected in the matrix. EPA does not interfere with the detection of nanozymes as colourimetric labels, but restricts the use of PMA for reducing the LOD. For the use of nanozymes' PMA, additional procedures of EPA elimination (i.e. washing of test strips [14,15], or enrichment of the target antigen using magnetic concentration [16]) were used. However, these additional procedures ruin the major advantages of LFIA (user-friendliness and rapidity). The proposed approach aims to eliminate the interference of EPA, thus providing a reduction of the LOD of LFIA.

We selected core@shell Au@Pt nanoparticles as nanozymes. This choice was dictated by high PMA [17], tunable optical properties [18], well-developed protocols of functionalization with receptor biomolecules [19] and a wide application in different bioanalytical assays (LFIA [20,9], barometer biosensors [21,22], homogenous assays based on the inhibition of PMA [23,24], modified ELISA procedure [19,25]). Because of their wide application as catalytic labels, the development of EPA inhibition protocols is especially actual.

This approach of EPA inhibition was performed on the matrixes with a high content of peroxidases and non-enzymatic substances with PMA—plant extracts and serum. The applicability of the approach for LFIA was demonstrated using the potato virus X (PVX) as a target. PVX is an important and worldwide spread pathogen that is controlled in tubers (seed materials) and leaves (in growing plants). Highly sensitive detection is mandatory for reducing economic losses caused by the PVX. Thus, LFIA with a low LOD is necessary for the routine, non-laboratory screening of latent infections.

Materials and methods

Materials

PVX was propagated in *Nicotiana tabacum* and isolated from the infected plants by Dr. Yu. A. Varitsev (A.G. Lorch All-Russian Potato Research Institute, Korenevo, Moscow region, Russia) following Goodman.[26] Polyclonal antibodies (Ab) against PVX were described in our previous publication.[27] Protein A from *Staphylococcus aureus* was purchased from Imtek, (Moscow, Russia). Tetrachloroauric (III) acid trihydrate, sodium hexachloroplatinate (IV) hexahydrate, nickel (II) sulphate hexahydrate, ascorbic acid (AA) sodium salt, trisodium citrate, sucrose, sodium dextran sulphate, 30% hydrogen peroxide, 3,3′–diaminobenzidine (DAB), 3,3',5,5'-tetramethylbenzidine (TMB), bovine serum albumin (BSA), horseradish peroxidase (HRP) and dimethyl sulfoxide (DMSO) were purchased from Sigma-Aldrich (St. Louis, USA, www.sigmaaldrich.com). All other salts, acids and alkalis were purchased from Chimmed (Moscow, Russia, www. chimmed.ru).

LFIA test strips were fabricated using nitrocellulose membranes CNPC-12, a conjugate release matrix (PT-R5), sample (GFB-R4) and absorbent pads (AP045) produced by Advanced Microdevices (Ambala Cantt, India, www.mdimembrane.com).

Synthesis of gold nanoparticles

Gold nanoparticles (GNP) were synthesized by the Frens method [28] with modifications. The solution of $HAuCl_4$ (1 mL, 1% w/v) was mixed with Milli-Q water (95 mL) in a flask equipped with a condenser and adjusted to the boiling point. Then, 4 mL of sodium citrate (1% w/v) was rapidly injected into the mixture. The mixture was boiled under vigorous stirring for 30 min.

Synthesis of Au@Pt nanoparticles

Synthesis of Au@Pt was performed following the protocol described by Gao et al. [14] with modifications. GNPs (60 mL) were mixed with Na_2PtCl_6 (12 mL, 10 mM) and 16 mL H_2O for 10 min at 80 ± 2 °C.; then AA (12 mL, 50 mM) was added using a peristaltic pump (rate 400 µL min^{-1}; 30 min). After the addition of AA, the mixture was stirred for another 30 min at 80 ± 2 °C.

Conjugation of nanoparticles with antibodies

The pH value of Au@Pt and GNP was adjusted to pH 9.0 by 0.2 M K_2CO_3. The aliquot of Ab (10 µg/mL) was added to the nanoparticles and incubated with gentle shaking for one hour at room temperature. Then, BSA was added to its final concentration equal to 0.1%. Nanoparticles were separated by centrifugation for 20 min at 12,000 g for Au@Pt and 20,000 g for GNP. Conjugates of Ab with Au@Pt (Ab-Au@Pt) and GNP (Ab-GNP) were redispersed in 20 mM Tris buffer pH 7.5 containing 0.25% BSA, 0.25% Tween-20 and 1% sucrose.

Measurement of PMA of Au@Pt, extracts and serum

The protocol for measurement of PMA of nanozymes was used.[29] All the solutions were prepared before use. The stock solution of TMB was prepared in DMSO (10 mM) and mixed with sodium citrate buffer (10 mM, pH 4.0) to the final concentration of TMB equal to 2 mM. Dilutions of H_2O_2 were prepared using Milli-Q water. The measurements were performed for Ab-Au@Pt, HRP, potato tuber, leaf extracts, and rabbit's serum. Sodium citrate buffer was used for the dilution of Ab-Au@Pt (1:100 V:V) and HRP (0.11 µg/mL). Tuber extract (1 g of tuber in 5 mL of 50 mM of potassium phosphate buffer with 0.05 M of NaCl (PBS) with 0.05% Triton X-100, pH 7.4 (PBST) was prepared by combining extracts from 15 different potato tubers. Leaf extract (1 g of leaves in 10 mL PBST) was prepared by combining leaves from 12 different potato plants. The obtained extracts were centrifuged (2 min, 5000 g), and the supernatants were used for further measurements.

Measurements of optical density at 650 nm (A_{650}) were performed using EnSpire Multi-mode Plate Reader (Perkin Elmer, USA). Aliquots of the extracts/Ab-Au@Pt (10 μL) were mixed with 40 μL H_2O_2 (0–9800 mM), and 50 μL of TMB (2 mM) was added. The values of A_{650} were recorded every 10 sec over 180 sec at 25 °C. All measurements were performed twice. The duration of the initial rate period was chosen after a linear fitting with the criterion $R^2 \geq 0.98$.[29] The initial rate ($\Delta A_{650}/\Delta t$) was calculated as a slope for the chosen linear interval. The initial rate was converted to the product concentration using a molar absorption coefficient 39,000 M^{-1} cm^{-1} for TMB.[29] Vmax and Km were calculated in OriginPro9 (Origin Lab, Northampton, MA, USA) using the Michaelis–Menten fitting function (y = Vmax * x / (Km + x)), where v_o values were on the y-axis and substrate concentration on the x-axis. Also, Vmax and Km were calculated using the Lineweaver–Burk plot (1/V=Km/Vmax*1/[S]+1/Vmax), where an intercept with y-axis corresponds to 1/Vmax, and the slope of linear fitting corresponds to Km/Vmax.

Transmission electron microscopy

Transmission electron microscopy (TEM) was carried out using the microscope Jeol JEM-1000 (Jeol, Tokyo, Japan, www.jeol.co.jp) operating at 80 kV. The aliquots (20 μL) of Au@Pt were incubated on a formvar-coated copper grid for 15 min. The excess liquid was carefully removed using filter paper, and grids were dried at 37 °C for 2 h. Digital images were analysed using Image Tool software (UTHSCSA, San Antonio, TX, USA).

Dynamic laser scattering and Zeta-potential measurement

The hydrodynamic diameters and zeta potentials of GNPs and Au@Pt nanoparticles were measured using the Zetasizer Nano (Malvern Panalytical, Malvern, UK, www.malvernpanalytical.com). The temperature was stabilized at 25 °C, and the scattering angle was 173 °. The statistical analysis ($n = 100$) was performed using the Malvern software ver. 7.11.

Test-strip preparation

The nitrocellulose membrane CNPC-12 was used as a working membrane. Protein A (0.5 mg mL−1) and Ab (1 mg mL−1) in PBS were dispended (0.15 uL per mm) using the IsoFlow dispenser (Imagene Technology, Hanover, USA) at the control and test zones (CZ and TZ, respectively) on the working membrane. Fiberglass membrane PT-R5 was soaked (1.5 uL per mm) with Au@Pt conjugates (200 mg L^{-1} based on Au concentration) or GNP conjugates (A_{520}=4.0). All membranes were dried at 30 °C for 24 h; then, the sample (GFB-R4) and absorbent pads (AP045) were glued. The assembled multimembrane composite was cut into strips (3.0 mm width) by an Index Cutter-1 (A-Point Technologies, Gibbstown, NJ, USA).

Preparation of potato tuber and leaf extracts

Both healthy and infected potato tubers and leaves were provided by Dr. Yu. A. Varitsev (A.G. Lorch All-Russian Potato Research Institute, Korenevo, Moscow region, Russia). All probes were tested preliminarily with qPCR and ELISA. Tubers and leaves were washed and thoroughly homogenized (1 g) in PBST (10 mL) with porcelain mortar for 1 min. To produce extracts with low PVX concentrations, the initial infected extracts were diluted with healthy extracts.

Lateral flow immunoassay

For plotting calibration curves, LFIA was performed in artificially contaminated extracts. PVX was added in the range of 0.125 μg/mL – 0.5 pg/mL. Healthy extracts were used for the dilution and as the negative control. Each concentration was measured in triplicate. Three formats of LFIA were performed. The first format (LFIA-1) used GNP as the label. The second and third formats (LFIA-2 and LFIA-3) used Au@Pt as the label. For LFIA-1 and 2, test strips were vertically submerged in the tested probes for 5 min. For LFIA-3, a Ni^{2+}-DAB-enhanced substrate solution consisted of 0.05% DAB, 200 mM H_2O_2, 0.05% $NiSO_4*7H_2O$ in 50 mM PBS, pH 7.3, and was dropped (20 μL) on the test strip after completion of LFIA-2. The substrate solutions were incubated on test strips for 5 min. After completion of LFIA-1–3, test strips were scanned using a Canon 9000F Mark II scanner (Canon, Japan, www.canon.com). The digital images of test strips in greyscale mode were analysed using the TotalLab TL120 software (Nonlinear Dynamics, UK). The calibration curves were plotted as a function of the mean colourimetric signal of the test zone against PVX concentration. The LOD of LFIA was calculated as a virus concentration corresponding to a colourimetric signal higher than a mean value for a negative control plus three standard deviations.

Results and discussion

Characterizations of nanoparticles

Synthesized Au@Pt possesses urchin-shaped morphology (Fig. 1). The formation of the spiky Pt layer on GNP seeds resulted in the increase of the hydrodynamic diameter from 22.2 ± 5.2 to 54.9 ±12.2 nm (Fig. S1A). Zeta-potential (Fig. S2) of Au@Pt (-25.0 ± 8.7 mV) was comparable to GNP (-28.7 ± 12.0 mV). The optical spectrum (Fig. S3) of Au@Pt significantly differs from the spectrum of initial GNP seeds. The growth of Pt layer resulted in the disappearance of the plasmonic resonance peak at 520 nm specific to GNP and in the significant increase of the absorbance in the whole UV-Vis wavelength range. The Au@Pt suspension had dramatically higher colouration in comparison with initial seeds GNP (Fig. S4). Results of TEM

confirm the formation of clusters of Pt-particles on the GNP seeds and the absence of the separate small Pt-particles.

Au@Pt nanoparticles and GNP were conjugated to the Ab using physical adsorption. Binding of the Ab to the surface resulted in an increase of the hydrodynamic diameter of particles to 77.6 ± 18.9 nm (Fig. S1B). The increase of the hydrodynamic diameter for 10–15 nm for Ab-Au@Pt was similar to the previously shown increase of the hydrodynamic size of GNP [30] and is explained by the formation of protein corona around Au@Pt nanoparticles. The observed increase of hydrodynamic diameters of particles confirms the absence of poly-layer adsorption of antibodies. Poly-layer adsorption is undesirable because it leads to the blocking of the nanozyme's surface and significantly reduces the PMA.[31] Protein corona consists of antibodies and BSA molecules and provides the stability of nanoparticles in the solution and antigen-binding properties. To take into account the effect of protein corona on PMA, Ab-Au@Pt was used instead of bare Au@Pt for its kinetics characteristics.

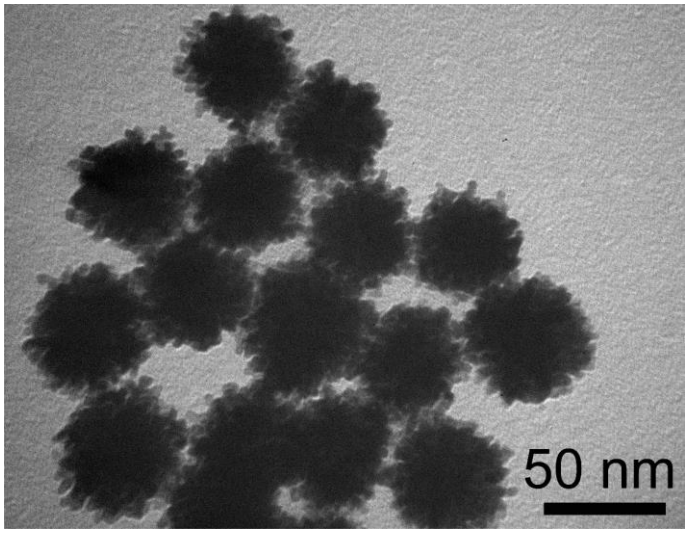

Fig. 1 Microphotograph of Au@Pt nanoparticles

Kinetic characterization of peroxidase-mimicking activity

For Ab-Au@Pt, the increase of H_2O_2 concentrations from 2 to 120 mM leads to a spike growth of v_0 from 0.33 to 1.33 μM/s. The further increase of H_2O_2 concentration did not significantly affect the initial velocity v_0 (Fig. 2); the inhibition by the substrate was not observed (Fig. S5). Calculated Km (5.75 mM) and Vmax (1.28 μM/s) values are in typical range for Pt-containing nanozymes (Table S1).

In opposition, peroxidases in potato tuber and leaf extracts as well as HRP (Figs. S6–S8) have a narrow range of optimal concentration of H_2O_2. The major growth of v_0 was observed within the range of 0.2 to 2 mM of H_2O_2. The ranges of concentration of H_2O_2 2–18 mM (tuber

extracts, Fig. S6B) and 2–12 mM (leaf extracts, Fig. S7B) resulted in reaching a plateau of the initial rate. The concentrations of the H_2O_2 higher than 20 mM led to the inhibition (Fig. 2) of EMA in both matrixes. The increase of H_2O_2 concentration to 200 mM results in the reduction of the initial rate up to 84% for tuber extracts and 77% for leaf extracts while maintaining a high PMA of Ab-Au@Pt (Fig. 2).

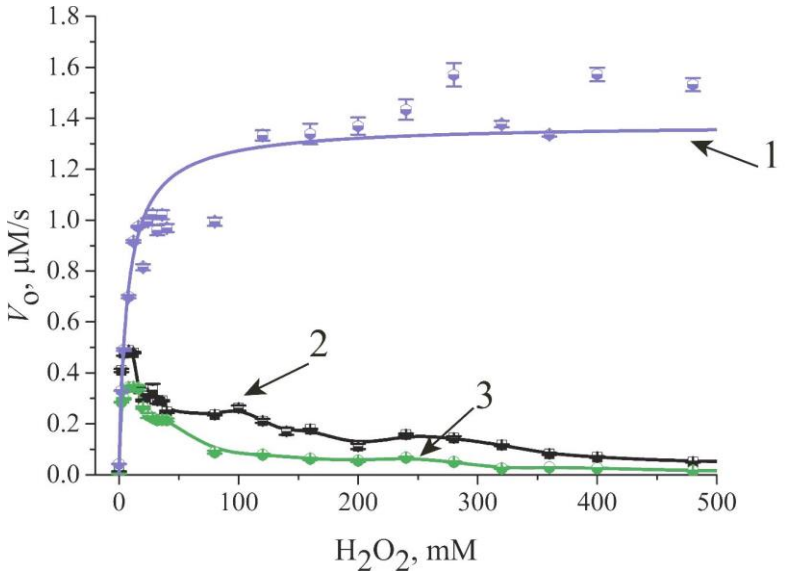

Fig. 2 The effect of hydrogen peroxide concentrations on the initial velocity. 1 – Ab-Au@P (1.5 pM); 2 – potato tuber extracts; 3 – potato leaf extracts.

The inhibition of peroxidases in extracts is explained by substrate inhibition and follows a similar mechanism described for HRP.[32] Inhibition of peroxidases in potato extracts required higher concentrations of H_2O_2 (12 and 18 mM for peroxidases in leaf and tuber extracts) in comparison with HRP (8 mM). This phenomenon could be explained by the different biochemical properties and stabilities of plant peroxidases.[33] Unlike the natural peroxidases where catalysis occurs on a single active group (heme) in a molecule, nanozymes' catalytic conversion proceeds on many active sites on the surface of nanozyme particles. The presence of multiple active centres on the surface of particles and a lower affinity to H_2O_2 (apparent values of Km for extracts are 12–15 times lower than for Ab-Au@Pt) may explain the higher stability of PMA in concentrated H_2O_2 solutions.

Based on the kinetics study, for LFIA we selected an H_2O_2 concentration equal to 200 mM. The selected concentration of H_2O_2 provided a condition for the selective detection of nanozymes, while the EPA of the extracts was inhibited and did not provide a significant contribution to the colourimetric signal (Fig. S9). Using H_2O_2 for the inhibition of EPA has some benefits compared with sodium azide—a widely used inhibitor of peroxidases. Sodium azide causes the inhibition of PMA of Au@Pt [18], thus reducing the efficiency of enhancement. In the

proposed approach, H_2O_2 plays a double role—both in the inhibition of EPA of matrixes and the detection of PMA of nanozymes. Thus, the fusion of these two stages into one step makes the whole procedure easier and less time-consuming. In the case of sodium azide, the stages of inhibition of EPA and detection of PMA are performed consistently, thus increasing the number of manipulations and the assay time. Considering these findings, we conclude that the proposed approach is applicable to the enhancement of LFIA.

Nanozymes of different chemical natures (i.e. metal-containing-Au@Pt [21], Pd-Ir [34], carbon-based [35]) demonstrate PMA at molar-millimolar range concentrations of H_2O_2. Thus, the proposed approach of EPA inhibition while maintaining PMA may be considered for a broad range of nanozymes and bioanalytical techniques.

To confirm the applicability of the proposed assay to the different matrixes, we studied the effect of H_2O_2 concentrations on the EPA of rabbit serum. The results (Fig. S17) demonstrate that for the inhibition of EPA in serum to occur, higher concentrations of H_2O_2 are required. The EPA was inhibited by an H_2O_2 higher than 35 mM, and the elimination of the EPA was observed at 1 M. Au@Pt nanozymes demonstrate a high PMA at 1 M of H_2O_2 (Fig. S5), which confirms the applicability of the proposed approach to the LFIA in different matrixes.

Development of lateral flow immunoassay

Three formats of LFIA were performed (Fig. 3). The performed LFIA used nanosized labels (GNP and Au@Pt) with different optical and catalytic properties. The comparison of LODs for LFIA-1 and LFIA-2 allows finding the influence of the label's optical properties on the LFIA's sensitivity. The comparison of LODs for LFIA-2 and LFIA-3 allows finding the influence of the PMA of Au@Pt on the LFIA's sensitivity. All three formats were based on the use of the same antibodies and test strips. The detection of the results for all three LFIAs was performed by the colourimetric signal (intensity of colouration) in TZ. The presence of PVX in the probe resulted in the formation of coloured TZ and CZ. The absence of PVX resulted in the colouration of CZ only. The colouration of CZ demonstrates the reliability of the assay. The treatment of test strips with H_2O_2 occurs after completion of the immunochemical reaction and thus does not interfere with affine binding and immune complex formation.

LFIA-1 was the conventional LFIA with GNP as the colourimetric label. Immune complexes were formed between PVX and Ab-GNP and further captured by Ab in the TZ. LFIA-2 was based on the same principle of immune complex formation as LFIA-1 but utilized Au@Pt as the colourimetric label. LFIA-3 was performed after completion of LFIA-2. LFIA-3 used PMA of Au@Pt for the conversion of the substrate to the product directly on the test strip. Accumulation of the insoluble product resulted in the increase of colourimetric signal.

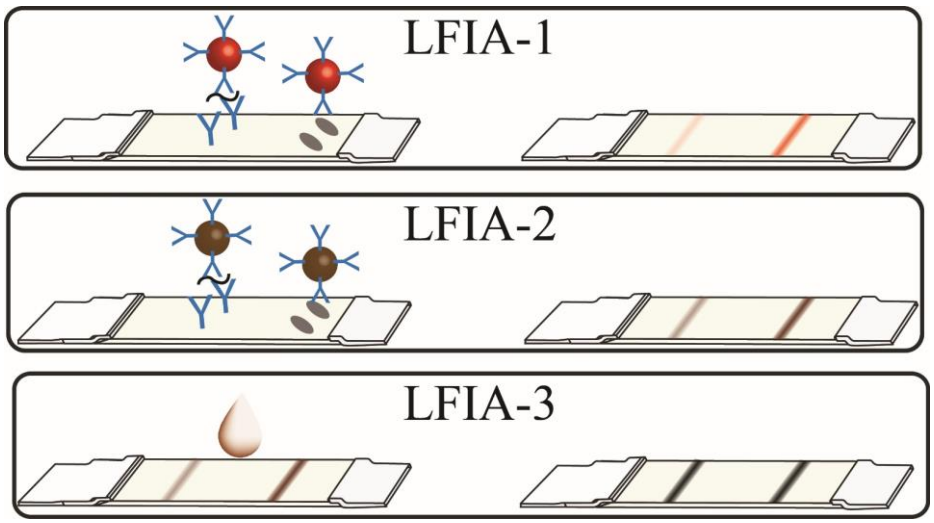

Fig. 3 Three formats of LFIA. Test strips after completion of LFIA-2 were used for LFIA-3. In LFIA-3, the addition of the substrate solution initiates catalytic reaction and accumulation of insoluble coloured product that significantly increase the colourations of TZ and CZ.

The LOD of LFIA-1 was 2 ng/mL in both tuber (Fig. 4 A, D) and leaf extracts (Fig. S14). The LOD of LFIA-2 was 500 pg/mL (Fig. 4B, D). Au@Pt demonstrated contrast dark-coloured TZ and CZ in comparison with red-coloured GNP and resulted in a 4-times lower LOD. Despite the higher colouration of Au@Pt compared with GNP (Fig. S3,4), the replacement of GNP with Au@Pt as the colourimetric label did not provide a significantly lower LOD. In previously published articles, authors also reported a moderate reduction of the LOD (2–10 times) for Au@Pt as a colourimetric label in LFIA (Table S2).

Further reduction of the LOD was achieved using the PMA of Au@Pt and detection of coloured product on a test strip. Three different substrates (catechol, Ni^{2+}-DAB, and insoluble TMB) were compared in terms of colourimetric signal enhancement (Fig. S10). Ni^{2+}-enhanced DAB provided the highest increase of the colourimetric signal and was selected for signal amplification for LFIA-3. Also, we used insoluble TMB as more stable substrate in comparison with DAB.

The LOD for TMB-enhanced LFIA was 31 pg/mL for tuber and leaf extracts (Figs. S11–13). Also, we observed the background staining for the blank probes that limited the LOD. The use of Ni^{2+}-DAB-as the substrate for LFIA-3 provided an LOD equal to 4 pg/mL in tuber extracts (Fig. 4 C, D) and 8 pg/mL in leaf extracts (Fig. S14).

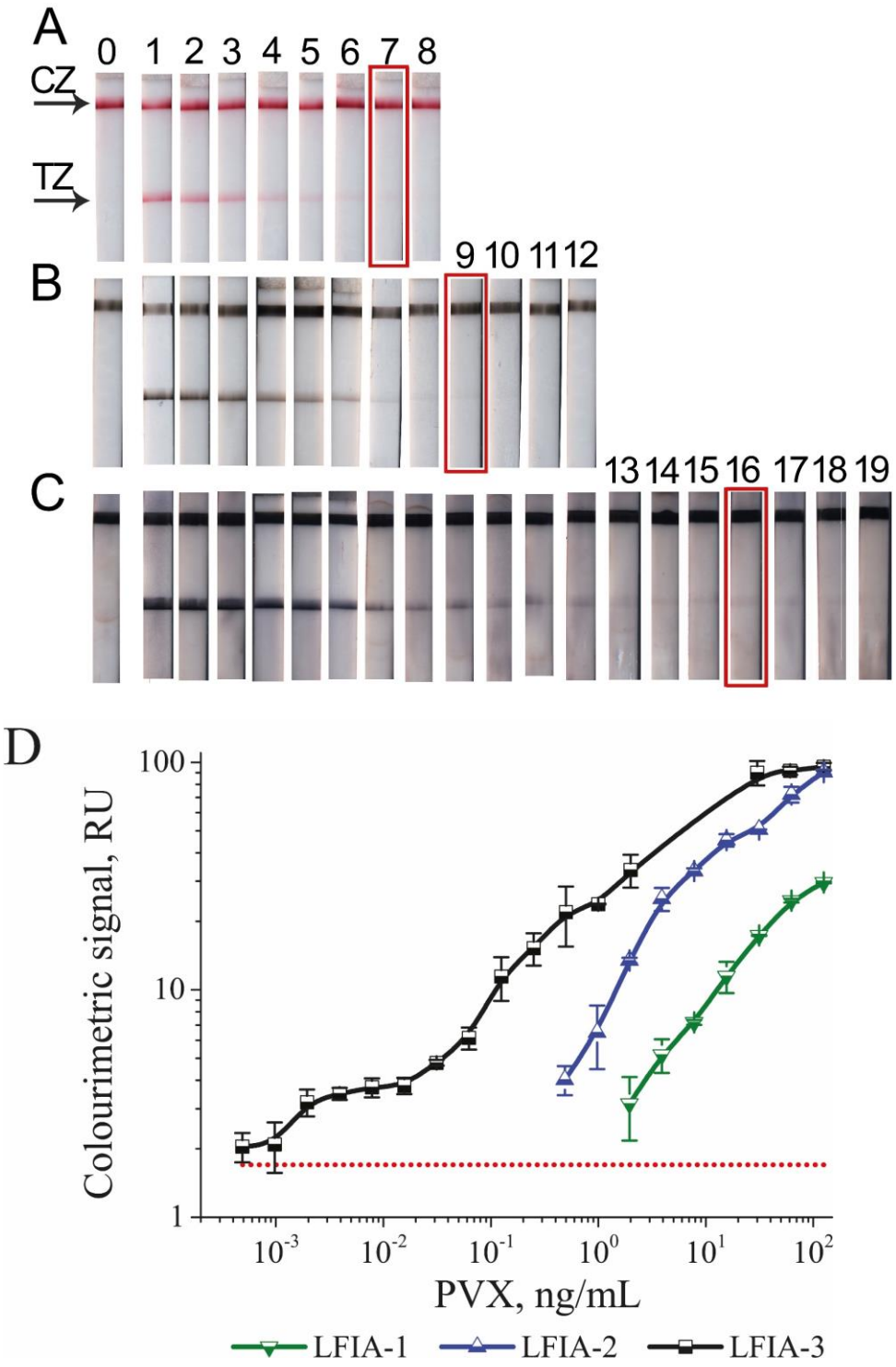

Fig. 4 LFIA-3 for the detection of PVX in tuber extracts. The test strips after: A – LFIA-1. B – LFIA-2. C – LFIA-3. D – Calibration curves for LFIA-1 – 3. Red dotted lines correspond to the background signal (1.7 RU). Numbers above the test strips correspond to the concentration of PVX, ng/mL: 1 – 125; 2 – 62.5; 3 – 31.2; 4 – 15.6; 5 – 7.8; 6 – 3.9; 7 – 2.0; 8 – 1.0; 9 – 0.5; 10 - 0.25; 11 – 0.125; PVX concentration, pg/mL: 12 – 63; 13 – 32; 14 – 16; 15 – 8; 16 – 4; 17 – 2; 18 – 1; 19 – 0.5; 0 – blank. Red frames around the test strips indicate the LOD values.

LFIA-3 demonstrated 125 and 62.5 times lower LODs in tuber and leaf extracts, respectively, in comparison with LFIA-2. In comparison with LFIA-1, the LOD values in tuber and leaf extracts were 500 and 250 times lower, respectively. Achieved LOD reduction is

comparable with a previously published enhancement using the PMA of nanozymes (Table S2). Achieved LODs of PVX in tuber and leaf are the lowest among other LFIA (Table S3).

Effect of H_2O_2 concentrations on the analytical characteristics of lateral flow immunoassay

To demonstrate the necessity of EPA inactivation for reaching a low LOD, we performed LFIA-3 with lower H2O2 concentrations equal to 9 mM (Fig. S15). Such lower concentrations did not inhibit peroxidases in leaf extracts. Endogenous peroxidases in the extract catalyse the reaction of the substrate conversion, leading to the formation of a grey blur along test strips (Fig. 15A). The non-specific colouration of blank probes restricted the efficiency of enhancement. The LOD of LFIA-3 with a low concentration of H_2O_2 was the same as for the second format (500 pg/mL).

Also, a significantly lower increase of colourimetric signal for probes with a high concentration of PVX (high initial colouration of TZ) was observed (Fig. 15B). This phenomenon may be explained by the competition for the substrate between Ab-Au@Pt and endogenous peroxidases. Considering lower Km value, the affinity of peroxidases to the substrate is higher. Thus, a lower number of the product is produced by nanozymes in TZ and CZ that resulted in the significantly lower increase of colourimetric signal after enhancement. Both these factors led to the inefficiency of catalytic enhancement by nanozymes for reaching lower LODs in the samples with high EPA.

In previous articles, authors also used elevated H_2O_2 (up to 10 M)[21] concentrations in the substrate solution for the detection of PMA of nanozymes in the different assays. However, elevated concentrations of H_2O_2 were not discussed as a tool for the inhibition of EPA. Gao et al. [36] employed dramatically different optimum values of H_2O_2 concentrations of irregular-shaped Pt nanoparticles (max. catalytic activity at 7.63 M H_2O_2) and HRP (max catalytic activity at 1.46 mM H_2O_2) for the ELISA-like detection of rabbit IgG. However, the choice of the elevated concentration of H_2O_2 was dictated by the selection of optimum condition for reaching a high speed of nanozyme's catalysed reaction and not by the inhibition of serum's EPA. Endogenous peroxidases of the rabbit serum were washed away with buffer prior to the addition of the substrate. Thus, summarizing these previously published results, we conclude that the application of H_2O_2 to the simultaneous inhibition of EPA and the detection of nanozymes for point-of-care assays was not shown.

Previously published articles utilized nanozymes with PMA and HRP as the catalytic labels and used different approaches for the elimination of EPA. Among these approaches, the most widely used was the washing of the test strip after the completion of the immunochemical reactions and before the addition of the substrate solution. This approach was applied for the LFIA of viral capsid protein of human immunodeficiency virus (p24) [9], prostate-specific antigen

[14] and rabbit IgG [20] in serum, *Escherichia coli* in milk [15] and pineapple juice [37], and cortisol in saliva [38]. For reducing the EPA effect, dilution of samples is also used.(i.e. serum samples were diluted from 10-times [39] to 20,000 times [40]). Enrichment of *Listeria monocytogenes* immunocomplexes with HRP-label by magnetic concentration from milk samples was reported.[16] However, all these approaches require additional stages of EPA elimination (washing and concentration), which complicate analysis and increase the time of the assay.

Developed in this article is an approach that combines in one-step the inhibition of EPA and detection of PMA of nanozymes directly on a test strip. However, this approach increases the assay time (by 5 min) and requires the use of a freshly prepared substrate solution. Both these requirements are drawbacks, especially for non-laboratory use. Nevertheless, the benefits of highly sensitive detection and the user-friendliness of the assay outweigh the drawbacks of the requirement for additional stages of the substrate addition and incubation.

Validation of lateral flow immunoassay

Validation of LFIA-1–3 was performed using potato leaves (n=24) and tubers (n=66). All used probes were without visible symptoms of infection. All probes were preliminarily tested with qPCR using commercially available kits. The presence of PVX was confirmed in 19 leaves probes and in 60 tubers probes (qualitative results are summarized in Table S4). The results of qualitative detection of PVX for LFIA-1–3 are summarized in Table 1. The colouration of TZs for LFIA-1–3 for analysed probes is depicted in Fig. S16. The results of testing demonstrate that LFIA-1 detected PVX in 16 leaves probes and 27 tubers probes. LFIA-2 detected PVX in 18 leaves probes and in 40 tubers probes. LFIA-3 detected PVX in 19 leaves probes and in 57 tubers probes.

Table 1 Quantitative results of LFIA-1–3 for the detection of PVX in leaf and tuber extracts. Number of positive/negative probes for every type of sample is shown in the bracket.

Assay	Probe type			
	Leaves		Tubers	
	Positive (19)	Negative (5)	Positive (60)	Negative (6)
LFIA-1	16	8	27	39
LFIA-2	18	6	40	26
LFIA-3	19	5	57	9

For all three formats of LFIA, no false-positive results were observed (Table 1). The sensitivity of LFIA-1 was 84% in leaf (16 from 19) and 45% in tuber (27 from 60) extracts. The use of a more efficient optical label (i.e. Au@Pt) instead of GNP provides higher sensitivity of LFIA-2—95% in leaf (18 from 19) and 67% in tuber (40 from 60) extracts. The use of the PMA

of Au@Pt provides higher sensitivity of LFIA-3—100% in leaf (19 from 19) and 95% in tuber (57 from 60) extracts. Three samples (# 41, 83, 84) with the presence of PVX were negative for all formats of LFIA. We hypothesise that this fact is explained by the concentration of PVX below the LOD even for LFIA with enhancement.

Conclusion

We developed the single-step approach for the detection of nanozymes with peroxidase-mimicking activity in the background of endogenous peroxidases. Steps of the endogenous peroxidase activity inhibition and Au@Pt peroxidase-mimicking activity detection were combined in a single 5-min stage, which ensures the applicability of the developed assay for non-laboratory analysis and provides 250-500 times lower limit of detection than conventional lateral flow immunoassay with gold nanoparticles.

However, despite the advantages of the reported approach, the applicability of nanozymes in lateral flow immunoassay remains limited by several factors. The first factor is non-specific binding of nanoparticles on porous membranes. After signal enhancement, such binding causes false-positive results of assays and limits their sensitivity. To reduce the non-specific binding of nanozymes, the optimizations of blocking buffer composition, concentrations of reagents and types of membranes will be required. The second factor is relatively low peroxidase-mimicking activity of nanozymes. The protein corona around nanozymes reduces peroxidase-mimicking activity by shielding the catalytic surface.[31] For lateral flow immunoassay, additional reduction occurs because of the trapping of nanozymes inside membrane pores.[41,42] To overcome the blocking, the surface of nanozymes can be recuperated by overgrowth with a bare catalytic layer over initial particles.[15] Similar methods of gold [41], silver [43] and copper [44] reduction over gold nanoparticle seeds were successfully used for highly sensitive assays without the peroxidase-mimicking activity use. We believe that the approach proposed by Fu et al. [15] of surface recuperation can improve the efficiency of nanozymes' use. *In situ* syntheses of nanozymes with high catalytic activity (such as Pt, Pd nanozymes) are also perspective tools for reaching lower limit of detection values.

Acknowledgments: The authors are grateful to Yu. A. Varitsev (A.G. Lorch All-Russian Potato Research Institute, Korenevo, Moscow region, Russia) for providing PVX and polyclonal antibodies to PVX, the infected and healthy plants

Funding information: This study was financially supported by the Russian Science Foundation (grant no. 16-16-04108).

Conflicts of interest: There are no conflicts to declare

References

(1) Wu, J.; Wang, X.; Wang, Q.; Lou, Z.; Li, S.; Zhu, Y.; Qin, L.; Wei, H. Nanomaterials with enzyme-like characteristics (Nanozymes): next-generation artificial enzymes (II). *Chem. Soc. Rev.* **2019**, *48* (4), 1004–1076. https://doi.org/10.1039/C8CS00457A.

(2) Wang, Q.; Wei, H.; Zhang, Z.; Wang, E.; Dong, S. Nanozyme: an emerging alternative to natural enzyme for biosensing and immunoassay. *TrAC Trends Anal. Chem.* **2018**, *105*, 218–224. https://doi.org/10.1016/j.trac.2018.05.012.

(3) Liu, J.; Xia, T.; Wang, S.; Yang, G.; Dong, B.; Wang, C.; Ma, Q.; Sun, Y.; Wang, R. Oriented-assembly of hollow FePt Nanochains with tunable catalytic and magnetic properties. *Nanoscale* **2016**, *8* (22), 11432–11440. https://doi.org/10.1039/c6nr00883f.

(4) Komkova, M. A.; Karyakina, E. E.; Karyakin, A. A. Catalytically synthesized Prussian blue nanoparticles defeating natural enzyme peroxidase. *J. Am. Chem. Soc.* **2018**, *140* (36), 11302–11307. https://doi.org/10.1021/jacs.8b05223.

(5) Liu, B.; Liu, J. Surface modification of nanozymes. *Nano Res.* **2017**, *10* (4), 1125–1148. https://doi.org/10.1007/s12274-017-1426-5.

(6) Huang, Y.; Ren, J.; Qu, X. Nanozymes: Classification, catalytic mechanisms, activity regulation, and applications. *Chem. Rev.* **2019**, *119*, 4357–4412. https://doi.org/10.1021/acs.chemrev.8b00672.

(7) Gao, L.; Zhuang, J.; Nie, L.; Zhang, J.; Zhang, Y.; Gu, N.; Wang, T.; Feng, J.; Yang, D.; Perrett, S.; Yan, X. Intrinsic peroxidase-like activity of ferromagnetic nanoparticles. *Nat. Nanotechnol.* **2007**, *2* (9), 577–583. https://doi.org/10.1038/nnano.2007.260.

(8) Kim, L. H. Y.; Plaza, K.; Thomas, S. R.; Draijer, C.; Radford, K.; Peters-Golden, M.; Mukherjee, M.; Nair, P. endogenous peroxidases in sputum interfere with horse-radish peroxidase-based ELISAs. *J. Immunol. Methods* **2018**, *454* (November), 76–79. https://doi.org/10.1016/j.jim.2017.11.005.

(9) Loynachan, C. N.; Thomas, M. R.; Gray, E. R.; Richards, D. A.; Kim, J.; Miller, B. S.; Brookes, J. C.; Agarwal, S.; Chudasama, V.; McKendry, R. A.; Stevens, M. M. Platinum nanocatalyst amplification: redefining the gold standard for lateral flow immunoassays with ultrabroad dynamic range. *ACS Nano* **2018**, *12* (1), 279–288. https://doi.org/10.1021/acsnano.7b06229.

(10) Kim, S. W.; Roh, J.; Park, C. S. Immunohistochemistry for pathologists: Protocols, pitfalls, and tips. *J. Pathol. Transl. Med.* **2016**, *50* (6), 411–418. https://doi.org/10.4132/jptm.2016.08.08.

(11) Radulescu, R. T.; Boenisch, T. Blocking endogenous peroxidases: a cautionary note for immunohistochemistry. *J. Cell. Mol. Med.* **2007**, *11* (6), 1419–1419.

https://doi.org/10.1111/j.1582-4934.2007.00185.x.

(12) Yang, H.; Xu, W.; Zhou, Y. Signal amplification in immunoassays by using noble metal nanoparticles: A review. *Microchim. Acta* **2019**, *186* (12), Article # 859. https://doi.org/10.1007/s00604-019-3904-9.

(13) Bishop, J. D.; Hsieh, H. V.; Gasperino, D. J.; Weigl, B. H. Sensitivity enhancement in lateral flow assays: A systems perspective. *Lab Chip* **2019**, *19* (15), 2486–2499. https://doi.org/10.1039/C9LC00104B.

(14) Gao, Z.; Ye, H.; Tang, D.; Tao, J.; Habibi, S.; Minerick, A.; Tang, D.; Xia, X. Platinum-decorated gold nanoparticles with dual functionalities for ultrasensitive colorimetric *in vitro* diagnostics. *Nano Lett.* **2017**, *17* (9), 5572–5579. https://doi.org/10.1021/acs.nanolett.7b02385.

(15) Fu, J.; Zhou, Y.; Huang, X.; Zhang, W.; Wu, Y.; Fang, H.; Zhang, C.; Xiong, Y. Dramatically enhanced immunochromatographic assay using cascade signal amplification for ultrasensitive detection of *Escherichia coli* O157:H7 in milk. *J. Agric. Food Chem.* **2020**, *68* (4), 1118–1125. https://doi.org/10.1021/acs.jafc.9b07076.

(16) Cho, I.-H.; Irudayaraj, J. Lateral-flow enzyme immunoconcentration for rapid detection of *Listeria monocytogenes*. *Anal. Bioanal. Chem.* **2013**, *405* (10), 3313–3319. https://doi.org/10.1007/s00216-013-6742-3.

(17) Gao, Z.; Tang, D.; Tang, D.; Niessner, R.; Knopp, D. Target-induced nanocatalyst deactivation facilitated by core@shell nanostructures for signal-amplified headspace-colorimetric assay of dissolved hydrogen sulfide. *Anal. Chem*. **2015**, 87 (19), 10153–10160. https://doi.org/10.1021/acs.analchem.5b03008.

(18) Panferov, V.G.; Safenkova, I.V.; Zherdev, A.V.; Dzantiev, B.B. Urchin peroxidase-mimicking Au@Pt nanoparticles as a label in lateral flow immunoassay: impact of nanoparticle composition on detection limit of *Clavibacter michiganensis*. *Microchim. Acta* **2020**, *187*, Article # 268. https://doi.org/10.1007/s00604-020-04253-3.

(19) Gao, Z.; Xu, M.; Lu, M.; Chen, G.; Tang, D. Urchin-like (gold core)@(platinum shell) nanohybrids: a highly efficient peroxidase-mimetic system for in situ amplified colorimetric immunoassay. *Biosens. Bioelectron.* **2015**, *70*, 194–201. https://doi.org/10.1016/j.bios.2015.03.039.

(20) Zhang, J.; Yu, Q.; Qiu, W.; Li, K.; Qian, L.; Zhang, X.; Liu, G. Gold-platinum nanoflowers as a label and as an enzyme mimic for use in highly sensitive lateral flow immunoassays: application to detection of rabbit IgG. *Microchim. Acta* **2019**, *186* (6), Article # 357. https://doi.org/10.1007/s00604-019-3464-z.

(21) Fu, Q.; Wu, Z.; Du, D.; Zhu, C.; Lin, Y.; Tang, Y. Versatile barometer biosensor based on

Au@Pt core/shell nanoparticle probe. *ACS Sensors* **2017**, *2* (6), 789–795. https://doi.org/10.1021/acssensors.7b00156.

(22) Xiao, M.; Shen, H.; Fu, Q.; Xiao, W.; Bian, H.; Zhang, Z.; Tang, Y. practical immune-barometer sensor for trivalent chromium ion detection using gold core platinum shell nanoparticle probes. *Analyst* **2018**, *143* (6), 1426–1433. https://doi.org/10.1039/C7AN02047C.

(23) Pan, N.; Zhu, Y.; Wu, L. L.; Xie, Z. J.; Xue, F.; Peng, C. F. highly sensitive colorimetric detection of copper ions based on regulating the peroxidase-like activity of Au@Pt nanohybrids. *Anal. Methods* **2016**, *8* (41), 7531–7536. https://doi.org/10.1039/c6ay01789d.

(24) Peng, C. F.; Pan, N.; Zhi-Juan, Q.; Wei, X. L.; Shao, G. colorimetric detection of thiocyanate based on inhibiting the catalytic activity of cystine-capped core-shell Au@Pt Nanocatalysts. *Talanta* **2017**, *175*, 114–120. https://doi.org/10.1016/j.talanta.2017.06.005.

(25) Jiao, L.; Zhang, L.; Du, W.; Li, H.; Yang, D.; Zhu, C. Au@Pt nanodendrites enhanced multimodal enzyme-linked immunosorbent assay. *Nanoscale* **2019**, *11* (18), 8798–8802. https://doi.org/10.1039/C8NR08741E.

(26) Goodman, R. M. Reconstitution of potato virus X *in vitro*. I. Properties of the dissociated protein structural subunits. *Virology* **1975**, *68* (2), 287–298.

(27) Panferov, V. G.; Safenkova, I. V; Varitsev, Y. A.; Zherdev, A. V; Dzantiev, B. B. Enhancement of lateral flow immunoassay by alkaline phosphatase: a simple and highly sensitive test for potato virus X. *Microchim. Acta* **2018**, 185, Article # 25. https://doi.org/10.1007/s00604-017-2595-3.

(28) Frens, G. Controlled nucleation for the regulation of the particle size in monodisperse gold suspensions. *Nat. Phys. Sci.* **1973**, *241* (105), 20–22. https://doi.org/10.1038/physci241020a0.

(29) Jiang, B.; Duan, D.; Gao, L.; Zhou, M.; Fan, K.; Tang, Y.; Xi, J.; Bi, Y.; Tong, Z.; Gao, G. F.; Xie, N.; Tang, A.; Nie, G.; Liang, M.; Yan, X. Standardized assays for determining the catalytic activity and kinetics of peroxidase-like nanozymes. *Nat. Protoc.* **2018**, *13* (7), 1506–1520. https://doi.org/10.1038/s41596-018-0001-1.

(30) Safenkova, I. V.; Slutskaya, E. S.; Panferov, V. G.; Zherdev, A. V.; Dzantiev, B. B. Complex analysis of concentrated antibody-gold nanoparticle conjugates' mixtures using asymmetric flow field-flow fractionation. *J. Chromatogr. A* **2016**, *1477*, 56–63. https://doi.org/10.1016/j.chroma.2016.11.040.

(31) McVey, C.; Logan, N.; Thanh, N. T. K.; Elliott, C.; Cao, C. Unusual switchable peroxidase-mimicking nanozyme for the determination of proteolytic biomarker. *Nano*

Res. **2019**, *12* (3), 509–516. https://doi.org/10.1007/s12274-018-2241-3.

(32) Nicell, J. A.; Wright, H. A model of peroxidase activity with inhibition by hydrogen peroxide. *Enzyme Microb. Technol.* **1997**, *21* (4), 302–310. https://doi.org/10.1016/S0141-0229(97)00001-X.

(33) Pandey, V. P.; Awasthi, M.; Singh, S.; Tiwari, S.; Dwivedi, U. N. A comprehensive review on function and application of plant peroxidases. *Biochem. Anal. Biochem.* **2017**, *06* (01), 1–16. https://doi.org/10.4172/2161-1009.1000308.

(34) Xia, X.; Zhang, J.; Lu, N.; Kim, M. J.; Ghale, K.; Xu, Y.; McKenzie, E.; Liu, J.; Ye, H. Pd-Ir core-shell nanocubes: a type of highly efficient and versatile peroxidase mimic. *ACS Nano* **2015**, *9* (10), 9994–10004. https://doi.org/10.1021/acsnano.5b03525.

(35) Chen, T. M.; Tian, X. M.; Huang, L.; Xiao, J.; Yang, G. W. Nanodiamonds as pH-switchable oxidation and reduction catalysts with enzyme-like activities for immunoassay and antioxidant applications. *Nanoscale* **2017**, *9* (40), 15673–15684. https://doi.org/10.1039/c7nr05629j.

(36) Gao, Z.; Xu, M.; Hou, L.; Chen, G.; Tang, D. Irregular-shaped platinum nanoparticles as peroxidase mimics for highly efficient colorimetric immunoassay. *Anal. Chim. Acta* **2013**, *776*, 79–86. https://doi.org/10.1016/j.aca.2013.03.034.

(37) Ren, W.; Cho, I.-H.; Zhou, Z.; Irudayaraj, J. Ultrasensitive detection of microbial cells using magnetic focus enhanced lateral flow sensors. *Chem. Commun.* **2016**, *52* (27), 4930–4933. https://doi.org/10.1039/C5CC10240E.

(38) Zangheri, M.; Cevenini, L.; Anfossi, L.; Baggiani, C.; Simoni, P.; Di Nardo, F.; Roda, A. A simple and compact smartphone accessory for quantitative chemiluminescence-based lateral flow immunoassay for salivary cortisol detection. *Biosens. Bioelectron.* **2015**, *64*, 63–68. https://doi.org/10.1016/j.bios.2014.08.048.

(39) Tian, M.; Xie, W.; Zhang, T.; Liu, Y.; Lu, Z.; Li, C. M.; Liu, Y. a sensitive lateral flow immunochromatographic strip with Prussian blue nanoparticles mediated signal generation and cascade amplification. *Sensors Actuators, B Chem.* **2020**, *309*, Article # 127728. https://doi.org/10.1016/j.snb.2020.127728.

(40) Fu, Q.; Wu, Z.; Li, J.; Wu, Z.; Zhong, H.; Yang, Q.; Liu, Q.; Liu, Z.; Sheng, L.; Xu, M.; Li, T.; Yin, Z.; Wu, Y. Quantitative assessment of disease markers using the naked eye: point-of-care testing with gas generation-based biosensor immunochromatographic strips. *J. Nanobiotechnology* **2019**, *17* (1), Article # 67. https://doi.org/10.1186/s12951-019-0493-z.

(41) Panferov, V. G.; Safenkova, I. V; Zherdev, A. V; Dzantiev, B. B. Post-assay growth of gold nanoparticles as a tool for highly sensitive lateral flow immunoassay. Application to

the detection of potato virus X. *Microchim. Acta* **2018**, *185* (11), Article # 506. https://doi.org/10.1007/s00604-018-3052-7.

(42) Mahmoudi, T.; Shirdel, B.; Mansoori, B.; Baradaran, B. Dual sensitivity enhancement in gold nanoparticle-based lateral flow immunoassay for visual detection of carcinoembryonic antigen. *Anal. Sci. Adv.* **2020**. https://doi.org/10.1002/ansa.202000023.

(43) Kim, W.; Lee, S.; Jeon, S. Enhanced sensitivity of lateral flow immunoassays by using water-soluble nanofibers and silver-enhancement reactions. *Sensors Actuators B Chem.* **2018**, *273*, 1323–1327. https://doi.org/https://doi.org/10.1016/j.snb.2018.07.045.

(44) Phan, L. M. T.; Kim, E. B.; Cheon, S. A.; Shim, T. S.; Kim, H.-J.; Park, T. J. Reliable naked-eye detection of *Mycobacterium tuberculosis* Antigen 85B using gold and copper nanoshell-enhanced immunoblotting techniques. *Sensors Actuators B Chem.* **2020**, *317*, Article # 128220. https://doi.org/10.1016/j.snb.2020.128220.